Input of fully 3D FE soil-structure modelling to the operational analysis of jack-up structures

Pisanò, Federico; Schipper, Robbin; Schreppers, Gerd Jan

DOI
10.1016/j.marstruc.2018.09.011

Publication date
2019

Document Version
Accepted author manuscript

Published in
Marine Structures

Input of fully 3D FE soil-structure modelling to the operational analysis of jack-up structures

Federico Pisanò[1]
Delft University of Technology
Geo-Engineering Section / Offshore Engineering Section
Stevinweg 1 – 2628 CN, Delft (Netherlands)

Robbin Schipper
Arup
Naritaweg 118 – 1043 CA Amsterdam (Netherlands)
(formerly TU Delft/DIANA FEA)

Gerd-Jan Schreppers
DIANA FEA
Delftechpark 19 – 2628 XJ Delft (Netherlands)

Abstract

Jack-ups are mobile structures widely employed in the offshore industry as drilling rigs or installation/maintenance vessels (e.g. for offshore wind farms). To assure safety at each location, *site-specific assessment* is required to predict the performance of the unit during installation and operations. The response of jack-ups to environmental loads is highly affected by the interaction between all footings (*spudcans*) and the underlying soil, an interaction still challenging to describe under general 3D loading.

This work emphasises the potential of 3D continuum simulations to capture non-linear soil-structural interaction in jack-up units. An integrated jack-up–spudcans-soil 3D finite element (FE) model is set up by including strain-hardening soil plasticity and geometrical non-linearity ($P-\Delta$ effects). After preliminary calibration of soil parameters, the FE model is successfully validated against literature results, namely obtained through (i) small-scale centrifuge experiments and (ii) numerical simulations based on macroelement foundation modelling. The validated FE model is then used to inspect several implications of soil modelling assumptions, as well as the response of the jack-up to relevant 3D loading combinations.

The results presented support 3D continuum modelling as a suitable approach to analyse spudcan fixity and, overall, the operational performance of jack-ups. Despite higher conceptual/computational difficulties, fully 3D simulations can valuably complement the insight from (rare) integrated physical modelling, and contribute to the improvement of soil-spudcan macroelement models.

Keywords: jack-up, spudcan, soil-structure interaction, site-specific assessment, soil plasticity, 3D finite element modelling.

[1]Corresponding author. E-mail: F.Pisano@tudelft.nl

1 Introduction

Jack-up structures play a prominent role in oil and gas developments as mobile offshore drilling units (MODUs) in shallow to moderate water depths. They are self-elevating structures, most usually comprising a triangular hull supported by three retractable lattice-work legs (Figure 1a). The primary advantage of the jack-up design is that it offers a steady and relatively motion-free platform in the drilling position, and mobilises quite quickly and easily. The use of jack-ups is not only limited to drilling operations as they can also serve diverse offshore construction/maintenance works, e.g. for offshore wind farms. When deployed as installation vessels, jack-ups usually come in smaller size and slightly different setups, possibly featuring more than three legs (Figure 1b)[2].

(a) mobile offshore drilling unit

(b) wind farm installation unit

(c) spudcan

Figure 1: Jack-up units in offshore developments.

Jack-ups are slender, dynamic-sensitive structures, whose global compliance under environmental loading is highly influenced by the interaction between the legs and the underlying soil. The jack-up legs are usually endowed with so-called *spudcan* footings (Figure 1c)[3], saucer-shaped polygonal or quasi-circular foundations with a central spigot and shallowly sloping conical underside (Randolph and Gourvenec, 2011). Being jack-ups by definition mobile units, a *site-specific assessment* is required for each new location to guarantee safe installation and operation. In the last decades, industry-academia partnerships have been promoted to develop reliable guidelines for site-specific assessment, including research programmes on geotechnical issues – e.g. the InSafe JIP (Osborne et al., 2009). The valuable knowledge generated in this area is collected, and continually updated, within the ISO 19905-1 document (Wong et al., 2012; ISO, 2016), originated from the previous SNAME 5-5A guidelines (SNAME, 2008; Hoyle et al., 2006).

The ISO standard comprises three acceptance check levels in order of increasing complexity

[2]The pictures in Figures 1a–1b are courtesy of GustoMSC (Schiedam, Netherlands).

[3]Picture from `http://www.emi.uwa.edu.au/news/uwa-team-investigate-new-footings-mobile-drilling-rigs-0`.

and reduced conservatism: a higher level of check is associated with more sophisticated foundation modelling, and advocated when lower acceptance criteria are not fulfilled. At the highest level – the so-called *Displacement Check* – the ISO standard requires finite element (FE) jack-up analyses including soil non-linearities and large deformation effects, so as to capture the consequences of foundation displacements through integrated soil-structure simulations (Wong et al., 2012; Purwana et al., 2012). As noted by Houlsby (2016), "*the important interaction at this stage is with structural engineers, who need to be able to analyse the forces in the structure, and for rather flexible structures such as jack-up units the structural forces depend critically on the foundation response*".

This work highlights the relevance of integrated 3D FE soil-foundation-structure modelling for the ISO Displacement Check (Level 3), with focus on the continuum simulation of non-linear soil-spudcan interaction. The ultimate goal is to strengthen the connections between lumped and fully 3D modelling of soil-spudcan interaction, so as to remedy the common dearth of specific field measurements and/or laboratory test results. However, the fully 3D soil–jack-up model has been developed in this spirit without attempting an "omni-comprehensive" modelling of all geotechnical factors, such as the influence of cyclic loading conditions (Vlahos et al., 2006) and partial pore water drainage (Ragni et al., 2016).

2 Modelling of spudcan fixity in jack-up structural analyses

Due to structural redundancy there is in jack-ups tight interaction between foundation response and structural demand, especially under extreme loading conditions. A typical issue in this context is the evaluation of the moment-rotation response at each spudcan, commonly referred to as *spudcan fixity*. To perform sound structural analyses, engineers must decide whether leg-seabed connections can be treated as pinned, fixed or deformable rotational constraints (Houlsby, 2016). The last, most realistic case is in fact quite hard to handle, as the overall spudcan-soil stiffness evolves during operations depending on multiple factors (e.g. soil type/behaviour, spudcan diameter, pore water drainage, effects of complex load combinations and loading cycles, etc.). It is known that uncoupled structural and geotechnical calculations cannot capture the global behaviour in presence of substantial soil non-linearities (Bienen and Cassidy, 2009; Cassidy et al., 2010); on the other hand, conceptual and computational difficulties arise when integrated soil-structure analyses are attempted.

The need for reliable fixity assessment has motivated over the years massive geotechnical research, as well as its gradual implementation into industry design guidelines (SNAME, 2008; ISO, 2016). Figure 2 summarises the main options available to analyse soil-spudcan interaction in operating jack-ups:

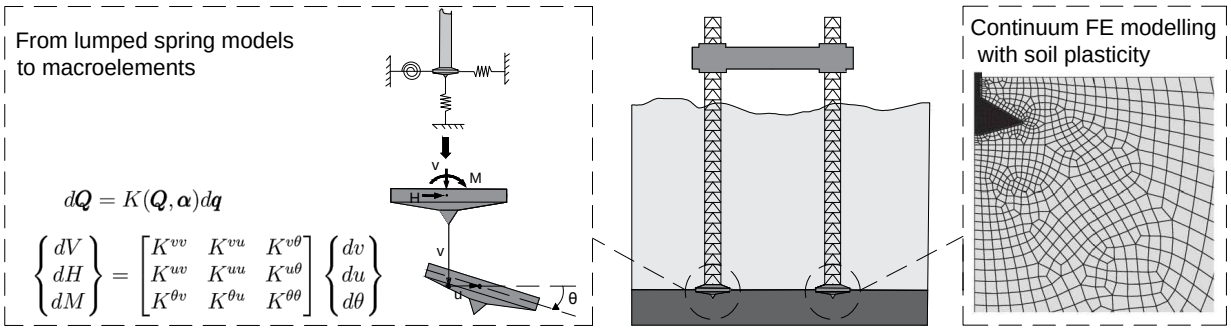

Figure 2: Lumped (left) vs continuum (right) modelling of soil-spudcan interaction.

– *continuum modelling* (Figure 2-right) – the spudcan and the soil are represented as parts of a 3D (or 2D) continuum domain. A wide range of modelling options are viable in terms of

soil behaviour (linear vs non linear), loading conditions (monotonic/static vs cyclic/dynamic), pore water drainage (drained, undrained or partially drained), kinematics (small vs large deformations), etc. Fixity analyses are mostly performed in this framework via non-linear FE computations, with complexity and computational costs determined by the whole set of modelling assumptions;

– *lumped modelling* (Figure 2-left) – soil-spudcan interaction can also be represented through lumped spring elements, i.e. through deformable rotational/translational constraints under each jack-up leg. Lumped soil-spudcan interaction results in remarkable computational savings, although condensing complex three-dimensional effects into a low number of force-displacement (and moment-rotation) relationships is often far from trivial.

As sketched in Figure 2–left, the lumped modelling of soil-spudcan interaction has developed further into *macroelement models* (sometimes termed *force-resultant models*). Formally, macroelements describe the foundation response through a generalised relationship between static (forces/moments) and kinematic (displacements/rotations) global variables (Georgiadis and Butterfield, 1988; Nova and Montrasio, 1991; Gottardi et al., 1999; Pisanò et al., 2014). In the relevant case of non-linear problems, such a relationship is formulated incrementally as:

$$\mathrm{d}\mathbf{Q} = \mathbf{K}\left(\mathbf{Q}, \boldsymbol{\alpha}\right) \mathrm{d}\mathbf{q} \tag{1}$$

where the vectors of static and kinematic variables – $\mathbf{Q}$ and $\mathbf{q}$, respectively – are related through the stiffness matrix $\mathbf{K}$. $\mathbf{K}$ emerges from the specific macroelement formulation with the following properties:

(i) the matrix is fully populated to capture all possible (constitutive) couplings among load components (6×6 components in general 3D problems);

(ii) the stiffness coefficients in $\mathbf{K}$ evolve during loading to reproduce non-linear interaction effects;

(iii) any material modelling framework can be applied to macroelements. In case of standard hardening plasticity, the $\mathbf{K}$ matrix depends on the current load vector $\mathbf{Q}$ and a set of evolving hardening variables (vector $\boldsymbol{\alpha}$ in Equation (1)), such as algebraic combinations of permanent displacement components.

Historically, the assessment of spudcan fixity gave the first input to the development of macroelement plasticity models (Schotman, 1989; Schotman and Efthymiou, 1989). Years later, other authors went deeper into modelling soil-spudcan interaction in both sand and clay (Martin and Houlsby, 2001; Houlsby and Cassidy, 2002; Zhang et al., 2014b), and started to incorporate macroelements into jack-up structural analyses (Dean et al., 1997b; Cassidy et al., 2001, 2002, 2004; Vlahos et al., 2008; Cassidy et al., 2010; Vlahos et al., 2011; Zhang et al., 2014a). A remarkable step forward was the extension to fully six-dimensional formulations (Bienen et al., 2006; Salciarini and Tamagnini, 2009; Tamagnini et al., 2013), that in turn enabled to analyse jack-ups under environmental loads of arbitrary orientation in the 3D space (Bienen and Cassidy, 2006, 2009). Although already popular in seismic applications (di Prisco and Pisanò, 2011), the generalisation of spudcan macroelements to cyclic loading has received far less attention (Vlahos et al., 2006); similarly, the application to non-standard spudcan shapes – e.g. skirted spudcans – has not yet been widely explored (Svanø and Tjelta, 1996; Cheng, 2015). These gaps stand out clearly in present industry guidelines (ISO, 2016), also in light of the very few measured data available about complete jack-up–soil systems – either from the field (Karunakaran et al., 1999; Nelson et al., 2000) or scaled laboratory tests (Dean et al., 1997a, 1998; Vlahos et al., 2005, 2008; Bienen et al., 2009; Cassidy et al., 2010).

In the authors' view, the macroelement modelling of soil-spudcan interaction can highly benefit from combining new experimental evidence and non-linear continuum simulations (Figure 2–right).

To date, the latter have been rarely applied to the fixity analysis of single spudcans, and even less to complete jack-up–spudcan–soil systems (Kellezi et al., 2007, 2008; Andresen et al., 2010). Fully 3D FE analyses based on hardening soil plasticity are proven hereafter a natural and effective approach to capture the structural behaviour of jack-ups.

3 3D FE jack-up–spudcans–soil modelling

The experimental and numerical results by Bienen et al. (2009) and Bienen and Cassidy (2009) provide precious (and rare) benchmarks for validating integrated jack-up–spudcans–soil models. These authors performed $200g$ centrifuge tests on the 1:200 physical model of a prototype jack-up having leg length, leg distance and spudcan diameter of 89 m, 25 m and 10 m, respectively. The centrifuge tests comprised in-flight installation, preloading and monotonic lateral pushover on dense silica sand (relative density $D_r = 84\%$). All load components (except torsion) were measured through strain gauges at the load reference points of each spudcan, as well as displacements along all six degrees-of-freedom at the hull reference point (HRP) – displacement transducers were not installed on single spudcans to limit instrumentation (Bienen et al., 2009).

Bienen et al.'s physical model was a simplified version of an average jack-up prototype, in which certain structural details (e.g. trusswork legs, leg-hull connections, etc.) where purposely overlooked to focus on global behaviour and foundation response. In the same spirit, a FE jack-up model has been developed here by taking the mechanical/geometrical properties of the model jack-up back to the (numerical) prototype scale. FE modelling and simulations have been entirely carried out by means of the software package DIANA (Manie, 2016).

3.1 Modelling of structural members

As the original physical model, the FE jack-up model is formed by a triangular hull and three legs (Figure 3a), each of them fitted with spudcan footings (Figure 3b) – geometrical/mechanical properties of the jack-up listed in Table 1:

- a rigid hull structure has been obtained by connecting six beams with square cross-section, as illustrated in Figure 3a and suggested by Bienen and Cassidy (2009). As a solid hexahedral hull was used in the original experiments, the mass density of the topside has been adjusted in the FE model to properly represent the hull mass/weight (see Table 1). Also the legs have been modelled through equivalent beams (no lattice trusswork), though with hollow circular cross-sections (Figure 3b) – in the ISO terminology this is referred to as *stick leg modelling* (ISO, 2016);
- the three supdcans have been modelled as 3D solid bodies to allow the continuum-based simulation of soil-foundation interaction. The geometry of each spudcan is detailed in Figure 3b (prototype scale) as in Bienen et al. (2009), with the only difference represented by the visible truncated tip. Keeping a sharp tip has negligible influence on the global response, but affects negatively the convergence of non-linear FE calculations due to high stress gradients;
- although the leg-hull connections of real jack-ups feature finite (non-linear) stiffness, perfectly rigid links have been set in the FE model in accordance with the reference physical model. Similarly, rigid leg-spudcan connections have been introduced in reasonable agreement with reality.

3.2 Modelling of sand behaviour

At variance with macroelement approaches (Section 2), continuum-based models aim to reproduce spudcan fixity from modelling soil behaviour at a lower scale. Accordingly, the adoption and cali-

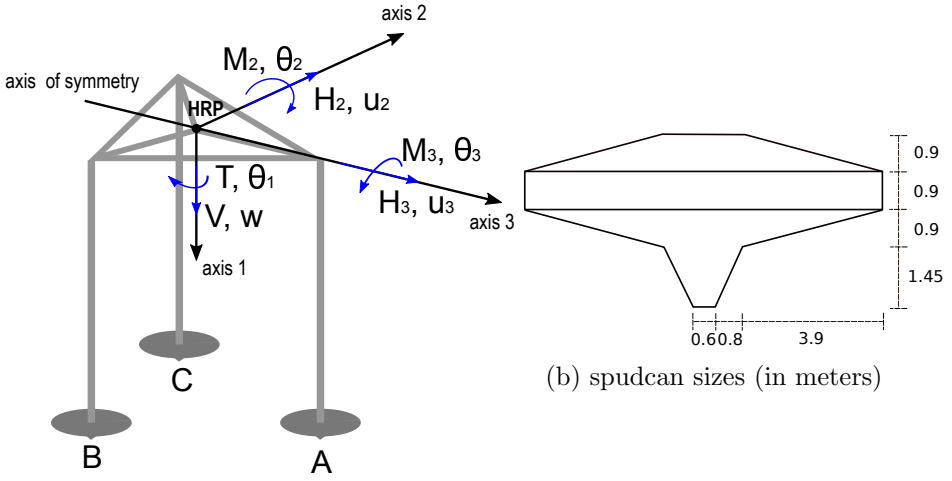

(a) hull, legs and spudcans

(b) spudcan sizes (in meters)

Figure 3: Structural components of the jack-up FE model.

Table 1: Geometrical and mechanical properties of the jack-up structure (prototype scale) – adapted from Bienen and Cassidy (2009)

Description	Value	Unit
Leg length	89	m
Centre of forward leg to centerline of aft legs	25	m
Centre to centre of aft legs	27	m
Cross-sectional area of each leg beam	2.9	m^2
Cross-sectional area of each hull beam	30	m^2
Second moment of area of each leg beam	7.04	m^4
Second moment of area of each hull beam	71.6	m^4
Mass density of each spudcan and leg beam	2700	kg/m^3
Diameter of each spudcan	10	m
Mass density of each hull beam	3400	kg/m^3
Young's modulus	200	GPa
Shear modulus	81	GPa

bration of suitable soil models is key to capturing the global performance of jack-up–spudcans–soil systems.

In this work, non-linear sand behaviour has been reproduced via the Modified Mohr-Coulomb (MMC) model available in DIANA (Groen, 1997; Manie, 2016), an elasto-plastic strain-hardening model derived from its simpler Mohr-Coulomb ancestor. In particular, the MMC model features (Nova, 2012): (i) pressure-dependent elastic moduli; (ii) two distinct non-linear yielding mechanisms for shear and radial (e.g. oedometric) loading paths; (iii) smooth shear strength variation across the whole Lode angle range, from triaxial compression to extension[4]; (iv) non-associated plastic flow rule, allowing for both volume contraction and dilation.

[4]The MMC formulation removes the sharp corners in the basic version of the Mohr-Coulomb yield/failure locus – such corners are in fact not physical and inconvenient to handle numerically.

3.2.1 The MMC model

The MMC constitutive equations are summarised in terms of usual isotropic (p') and deviatoric (q) stress invariants (Nova, 2012). First, the model features a non-linear (hypo-)elastic law, with constant Poisson's ratio ν and pressure-dependent bulk modulus (thus pressure-dependent Young's and shear moduli as well):

$$K = K_{ref} \left(p'/p'_{ref}\right)^{1-m} \tag{2}$$

where m and K_{ref} are constitutive parameters and $K\left(p' = p'_{ref}\right) = K_{ref}$ at the reference effective mean pressure p'_{ref}. Two distinct yielding mechanisms are accounted for through the yield functions f_1 (shear yielding) and f_2 (yielding cap for radial loading paths):

$$f_1 = \frac{q}{R_1(\theta)} - \frac{6\sin\phi}{3-\sin\phi}p' \qquad f_2 = p'^2 + \alpha\left(\frac{q}{R_2(\theta)}\right)^2 - p_c^2 \tag{3}$$

where α is a cap shape parameter, whereas the functions R_1 and R_2 determine the deviatoric section (i.e. dependence on the Lode angle θ) of the yield loci $f_1 = 0$ and $f_2 = 0$:

$$R_1(\theta) = \left(\frac{1-\beta_1\sin 3\theta}{1-\beta_1}\right)^n \qquad R_2(\theta) = 1 \tag{4}$$

with β_1 and n additional constitutive parameters. The mobilised friction angle at yielding, ϕ in Equation (3), evolves as a non-decreasing function of the equivalent plastic strain γ^p_{eff} (second invariant of the deviatoric plastic strain tensor):

$$\sin\phi = \sin\phi_f - (\sin\phi_0 - \sin\phi_f)\, e^{-a\gamma^p_{eff}} \tag{5}$$

where ϕ_0 and ϕ_f are the mobilised friction angle at first yielding and failure, respectively, while a is a material hardening parameter. The cap locus $f_2 = 0$ accounts for volumetric strain hardening, with its size governed by the hardening variable p_c and its evolution law:

$$\frac{\mathrm{d}p_c}{p_c} = \frac{1+e}{\gamma}\mathrm{d}\varepsilon^p_{vol} \tag{6}$$

in which ϵ^p_{vol}, e and γ are the incremental volumetric plastic strain, the current void ratio and an additional hardening parameter, respectively. Same as for yielding, distinct plastic flow mechanisms are introduced through two plastic potential functions, g_1 and g_2:

$$g_1 = q - \frac{6\sin\psi}{3-\sin\psi}p' \qquad g_2 = p'^2 + \alpha q^2 - (p^g_c)^2 \tag{7}$$

The dilatancy angle ψ in g_1 may be set at a constant value or evolve with the mobilised friction angle ϕ according to the well-known Rowe's relationship (Rowe, 1962):

$$\sin\psi = \frac{\sin\phi - \sin\phi_{cv}}{1-\sin\phi\sin\phi_{cv}} \tag{8}$$

where ϕ_{cv} is the constant volume friction angle observed e.g. in triaxial laboratory tests.

More details about the formulation and performance of the MMC model can be found in Groen (1997). Overall, the MMC formulation enhances significantly the monotonic performance of the standard Mohr-Coulomb model, previously employed by Kellezi et al. (2007, 2008) for continuum fixity analyses. However, due to the lack of a kinematic hardening mechanism, the MMC model would be intrinsically unsuitable to reproduce the cyclic behaviour of sands. Future work on the cyclic performance of jack-ups will require further enhanced soil models, formulated, for instance, in the framework of bounding surface plasticity, multi-surface plasticity, hypoplasticity or hyperplasticity (Dafalias and Manzari, 2004; Elgamal et al., 2003; Niemunis and Herle, 1997; Houlsby et al., 2017; Liu et al., 2018) – see e.g. recent applications of 3D FE hydro-mechanical modelling to offshore wind turbines (Corciulo et al., 2017; Kementzetzidis et al., 2018).

3.2.2 Calibration of sand parameters

MMC parameters have been identified for the silica sand used in the experiments of Bienen et al. (2009) – and in most centrifuge tests performed at the University of Western Australia (UWA). For this purpose, the laboratory test results available in Pucker et al. (2013) and Cheong (2002) have been exploited to model the monotonic behaviour of the material.

In Figure 4a the experimental curve from an oedometer compression test (Pucker et al., 2013) is compared to the corresponding MMC simulation (vertical compression with prevented lateral expansion). Despite the "irregular" experimental response recorded during unloading-reloading, the vertical stress-strain MMC performance seems satisfactory over a wide stress range (up to 1 MPa), owing to the combination of cap yielding mechanism (Equations (3)-right and (6)) and pressure-dependent elastic moduli (Equation (2)). Accurate confined compressibility is important up to even large soil stresses, such as those induced by the leeward spudcans of laterally-loaded jack-ups (see Section 4.1). However, the different relative densities D_r of the soil samples used in centrifuge experiments ($D_r = 84\%$, Bienen et al. (2009)) and oedometer tests ($D_r = 75\%$, Pucker et al. (2013)) should be mentioned.

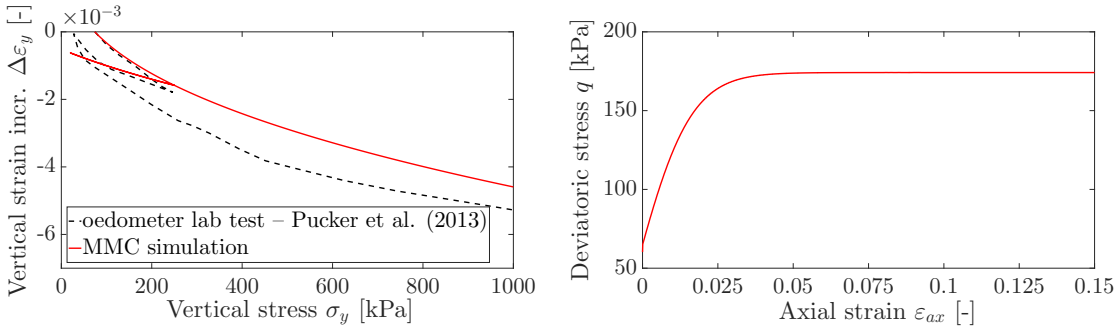

(a) oedometer test – laboratory test data from Pucker et al. (2013)

(b) triaxial test – MMC simulation based on data from Pucker et al. (2013) and Cheong (2002)

Figure 4: MMC model calibration for the UWA sand.

More drastic simplifications have been accommodated in terms of shear behaviour, due to the dearth of laboratory data and certain limitations of the MMC model. In fact, the MMC parameters governing such behaviour could not be univocally identified because: (i) Pucker et al. did not perform triaxial tests on sand specimens as dense as in Bienen et al. (2009); (ii) the same authors did not report about the volumetric response of the sand (dilatancy); (iii) the MMC shear hardening rule (5) cannot reproduce the strain-softening of medium-dense/dense sands. In light of these uncertainties/limitations, the following simplifying assumptions have been introduced:

- the hardening parameter a in Equation (5) has been calibrated for full strength mobilisation at approximately 5% axial strain (as shown in Pucker et al. (2013));
- with no speficic information about the strain-softening rate, the ultimate friction angle ϕ_f in Equation 5) has been set equal to the constant-volume strength found by Cheong (2002) via direct shear tests on the same UWA sand);
- nil dilatancy angle, unrealistic but compatible with the setting of constant-volume friction angle.

Figure 4b illustrates the simulated response to triaxial compression as resulting from the above constitutive assumptions (initial horizontal and vertical stresses equal to 120 and 60 kPa, i.e. initial $q = 60$ kPa). All MMC parameters in Table 2 have been set prior to 3D FE simulations, with

no later adjustments. All FE results presented in the following can be thus regarded as "class A" continuum-based predictions, similarly to the predictions obtained by Bienen and Cassidy (2009) via macroelement modelling.

Table 2: Calibrated MMC sand parameters

K_{ref}	p'_{ref}	m	ν	ϕ_0	ϕ_f	α	β_1	n	a	γ	ψ	γ_{dry}
[MPa]	[kPa]	[-]	[-]	[deg]	[deg]	[-]	[-]	[-]	[-]	[-]	[deg]	[kN/m^3]
110	100	0.75	0.3	18.5	33.75	0.222	0.75	-0.229	120	0.0008	0	17.36

The assumed combination of shear strength and dilatancy is expected to mobilise the most conservative performance of the FE model, to an extent depending on how fast the real sand transits from peak to constant-volume regime during foundation loading. Further, modelling soil softening would add undesired complexity to the "demonstrative" simulations performed in this study: it is well-known that the (likely) occurrence of strain localisation in brittle materials jeopardises the objectivity of numerical results and causes pathologic mesh dependence – i.e. lack of convergence upon mesh refinement (De Borst et al., 1993).

3.2.3 Soil-spudcan interface properties

The continuum analysis of soil-spudcan interaction requires the definition of suitable interface behaviour, so as to avoid unrealistic bonding between sand and spudcan steel. For this purpose the contact surface between the solids have been discretised through zero-thickness interface elements (Goodman et al., 1968). Their mechanical behaviour is expressed by a constitutive law relating interface stresses (normal and tangential) to the relative displacements between the two sides of the interface (split nodes).

In this work elastic/no-tension elements have been introduced to describe the soil-spudcan interface behaviour, with normal (compressive) and shear stiffnesses equal to $4 \cdot 10^6$ and $4 \cdot 10^5$ kN/m^3, respectively (see Manie (2016) for details about the selection of interface stiffness values). As shown later in Section 4, the soil-spudcan detachment allowed by no-tension interfaces is very relevant to pushover simulations. Conversely, enhancing interface elements with Coulomb frictional behaviour appeared unnecessary after preliminary FE tests – not reported for brevity: these tests showed that the jack-up response is nearly insensitive to interface shear strength limits, while adding interface friction proved detrimental for the convergence performance of the non-linear FE model.

3.3 Modelling of geometrical non-linearity

The behaviour of flexible structures such as jack-ups can hardly be captured through small deformation analyses (Nelson et al., 2000; Bienen and Cassidy, 2006). When the unit displaces significantly under external loading there are at least two relevant structural effects to consider (ISO, 2016):

- the lateral displacement of the hull induces gradual eccentricity of vertical loads and thus an increase in the global overturning moment (global $P-\Delta$ effects);
- the Euler amplification of local member forces increases the stresses within steel members (local $p-\delta$ effects).

$P-\Delta$ effects and foundation behaviour are intimately related, as the structural response depends on spudcan settlements/rotations and viceversa.

As suggested by the ISO 19905-1 standard, large displacement analyses can serve the analysis of displacement-dependent effects in jack-ups. In this work, the formulation and solution of the continuum problem is based on the so-called Total Lagrangian approach (Bathe, 1982), enabling the

combination of both material and geometrical non-linearities ($P-\Delta$ and $p-\delta$ effects). The Total Lagrangian framework is suitable in presence of large displacements/rotations and small strains, and relies on stress/strain measures defined with reference to the initial undeformed geometry. In particular, second Piola-Kirchhoff stresses are adopted as energy-conjugated counterparts of Green-Lagrange strains, whereas stress rates are measured through objective Jaumann rates (Holzapfel, 2000).

3.4 FE discretisation and simulation

Figure 5 depicts the whole 3D model after FE discretisation. All jack-up beams have been discretised through three-node Timoshenko elements (*class-III* beam elements, 24 integration points (Manie, 2016)), while a hybrid mesh of second-order tetrahedral/hexahedral elements has been generated for the three spudcans and the soil – in total, 36258 elements and 97931 nodes. As documented in Appendix A, the FE discretisation has been performed with special attention to trading off accuracy and computational costs. On average, run-times of approximately 3 hours have been recorded for the mesh in Figure 5 with parallel computations on 8 cores[5].

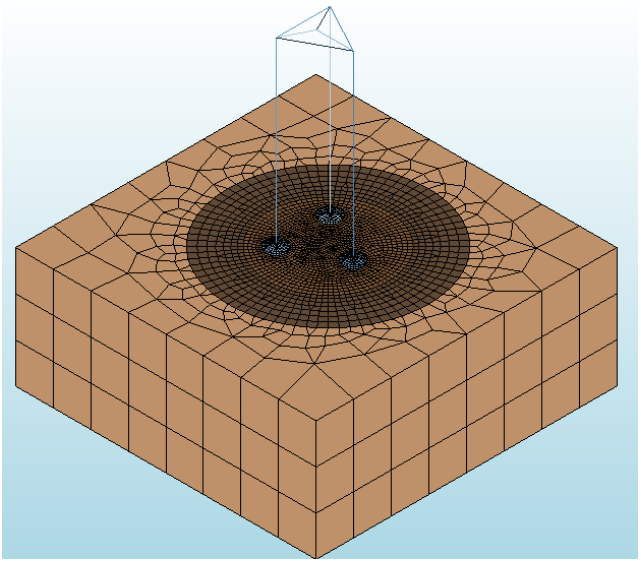

Figure 5: FE mesh of the jack-up–spudcans-soil 3D model.

Permanent boundary conditions include horizontal/normal supports along the lateral surface of the soil box in Figure 5, as well as full fixity of the whole bottom side. As for initial conditions, no attempts to simulate spudcan penetration have been made. Conversely, the traditional "wished-in-place" approach has been followed by initially setting full penetration for all spudcan undersides, in agreement with the experimental measurements from Bienen et al. (2009) (measured penetration of spudcan tips equal to 2.35 m). Along with the abovementioned simplifications, perfectly drained soil-spudcan interaction has also been assumed. Although debatable in offshore environments at the considered penetration level, such assumption is consistent with the reference physical model, tested on dry sand and widely exploited for the validation of the 3D FE model.

All FE simulations have been performed through the following loading stages:

1. Gravity loading – generation of initial stresses, first within the soil and then with the additional self-weight of the structure. At the end of this stage, all spudcans are equally compressed by a force V_{sw};

[5]Workstation specifications: Dell PowerEdge T620 2 * Intel® Xeon® Processor E5-2667 v2 25M Cache, 3.30 GHz, 8 cores.

2. Preloading – application of a vertical force on the topside to reproduce jack-up preloading (in practice achieved by pumping water into ballast tanks). At the end of this stage, spudcan compression equals $V_0 > V_{sw}$;

3. Unloading – preloading removal through the application of a suitable upward force. The stage-1 load V_{sw} is thus re-established on all spudcans;

4. Horizontal push-over – after re-initialising all displacements, lateral jack-up pushover by enforcing a horizontal load at the hull level.

Given the material and geometrical non-linearities in the FE model, all above loading stages have been solved incrementally based on the Newton-Raphson iteration scheme in its standard version (Bathe, 1982). The integration of MMC constitutive equations at each Gauss point is performed in DIANA via an implicit backward Euler algorithm with return-mapping (Simo and Hughes, 1998).

4 Validation against previous physical and numerical modelling

In this section the continuum 3D FE model is validated against the centrifuge test results and the macroelement-based simulations by Bienen et al. (2009) and Bienen and Cassidy (2009). As in the two reference studies, static/monotonic pushover has been exclusively considered by subjecting the structure to horizontal loads oriented as in Figure 6: the first case concerns loading along the symmetry axis of the hull (axis 3), whereas "misaligned" pushover with $\omega = 22°$ is considered in the second case to explore the fully 3D performance of the structure[6] (Bienen and Cassidy, 2006).

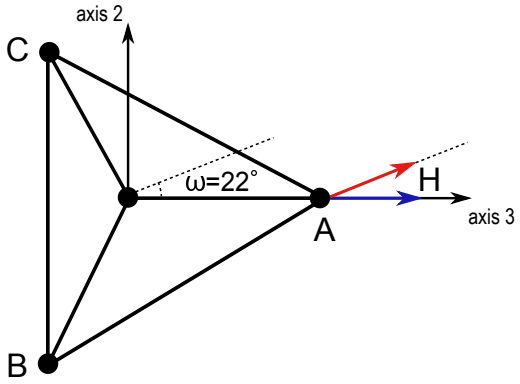

Figure 6: Orientation of the lateral loads in validation pushover analyses.

The outcomes of the continuum FE model are compared hereafter to experimental and macroelement-based results as reported by Bienen and Cassidy (2009). In agreement with the reference study, the above loading stages 1-3 have been set up to obtain V_0 =125.1 MN and V_{sw} =54.2 MN after vertical pre-loading and unloading, respectively.

4.1 Symmetric lateral pushover – $\omega = 0°$

The quality of continuum-based FE predictions in comparison to experimental (EXP) and macroelement (ME) results can be appreciated in Figure 7. Figure 7a gives an impression of the good agreement among EXP, ME and FE results in terms of global load-displacement response (i.e. recorded at the hull along axis 3). More specifically, the following observations can be drawn:

[6]Loads are applied at the hull-leg A connection point as in the reference centrifuge tests.

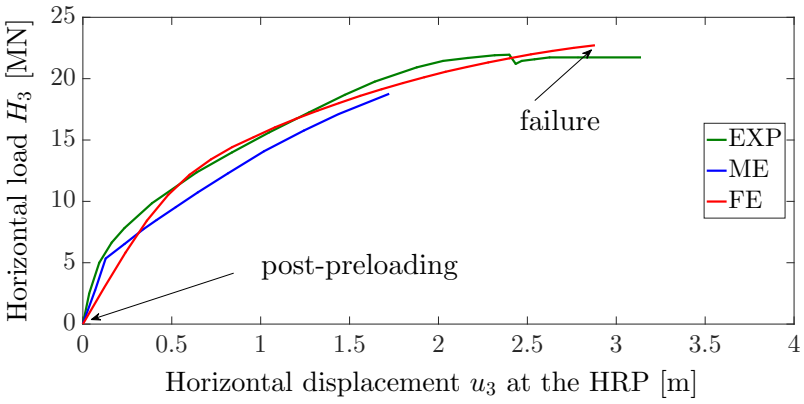

(a) horizontal force-displacement response at the hull – comparison among EXP, ME and FE results

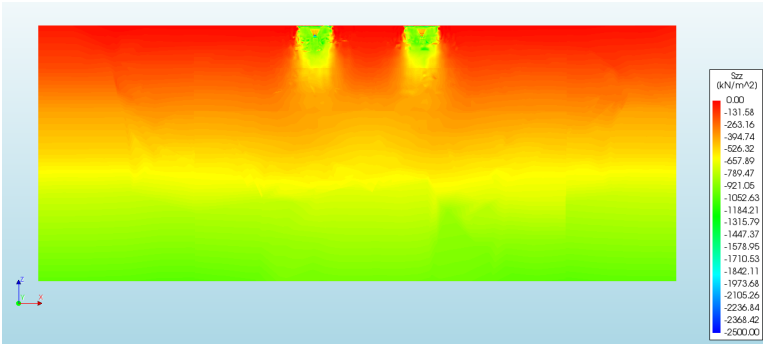

(b) vertical soil stress contours – after preloading

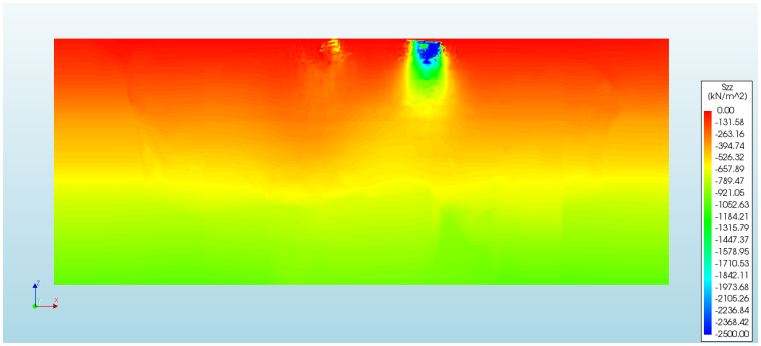

(c) vertical soil stress contours – at failure

Figure 7: Jack-up performance under symmetric lateral pushover.

– the load-controlled FE simulation attains failure (no convergence of Newton-Raphson iterations) at an applied load of 22.7 MN. This value compares to the experimental capacity (22 MN)[7] better than the corresponding ME prediction (18.8 MN);

– since soil plastifications occur under all spudcans from the onset of loading, the continuum FE curve exhibits a smooth decrease in stiffness during pushover. This is at variance with the sharp yielding produced by the ME simulation, arising from the elastic-plastic transition in the lumped interaction model;

– the FE curve features a lower initial (post-proloading) stiffness than the EXP and ME counter-

[7]The slight softening visible in the EXP curve is a peculiar experimental outcome, not captured by ME/FE results.

pats. Part of such discrepancy may be attributed to uncertainties/inaccuracies in the calibration of the MMC model (Section 3.2.2), however not fully sufficient to explain the observed difference. This matter is further discussed in Appendix B by considering the vertical load-settlement response of a single spudcan.

As confirmed by the vertical stress contours in Figures 7b–7c, the FE model captures correctly the dominant push-pull mechanism involving all spudcans: the leeward leg pushes spudcan A into the soil (note the high vertical stresses in Figure 4a, in excess of 2 MN), while the pulling of the windward legs determines stress relief under both spudcans B and C until failure (Figure 7c). At the onset of failure, the vertical stress is (close to) zero for a significant volume of soil under the windward legs, which is a clear precursor of foundation uplift-moment failure. From a numerical standpoint, milder convergence criteria could have let the FE simulation run slightly further at the expense of accuracy.

Figure 8 highlights the quantitative relevance of geometrical non-linearity. The load-displacement curve obtained in the Total Lagrangian large displacement framework (LDFE) is compared to, and found more accurate than, the corresponding small displacement prediction (SDFE): it is apparent that neglecting geometrical non-linearity can largely affect the evaluation of both lateral stiffness and ultimate capacity.

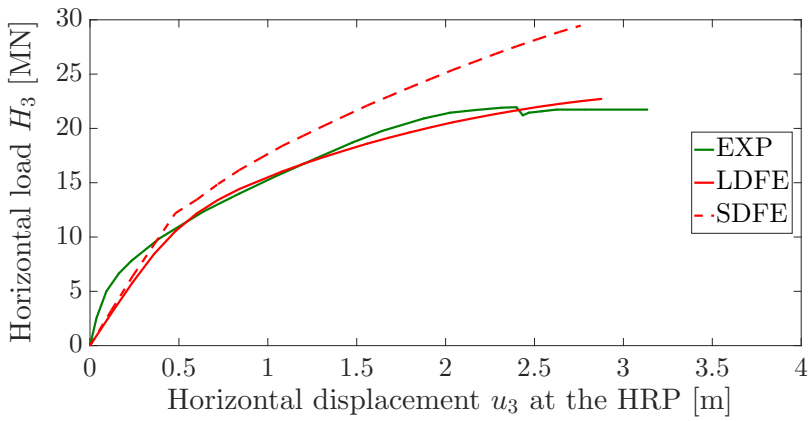

Figure 8: Influence of geometrical non-linearity on the jack-up response to symmetric pushover.

The experimental measurements from Bienen et al. (2009) also allow to validate the continuum FE model with respect to local spudcan responses. Figure 9 shows for all spudcans the comparisons among EXP, ME and FE results in terms of normalised horizontal-vertical ($H_3/V_0 - V/V_0$, Figure 9a) and moment-vertical ($M_2/DV_0 - V/V_0$, Figure 9b) load paths. Figure 10 displays the same comparisons for the corresponding force-displacement (Figures 10a–10b) and moment-rotation (Figures 10c–10d) responses (displacements and rotations are referred to the HRP). It should be noted that the EXP curves associated with spudcans B and C do not coincide because of initial uneven penetrations and vertical loads over the three footings (Bienen et al., 2009); further, Bienen et al. reported that all local measurements on spudcan A terminated quite earlier than for spudcans B-C due to the bending gauges exceeding their capacity before the global jack-up collapse.

Overall, the continuum FE model can properly reproduce the response of all spudcans, often in better agreement with EXP measurements than ME results. The different behaviours predicted for spudcans A and B-C are consistent with the aforementioned push-pull mechanism, including the counter-intuitive decreases in moment M_2 while the global pushover response is still hardening – compare Figure 7a to 10c–10d. At the last converged calculation step, $\mathrm{d}H_3/\mathrm{d}u_3$ at the HRP is about to vanish in response to the evolution of the two moment-resisting mechanisms in Figure 11a, namely vertical push-pull and local spudcan moments. Figure 11b explains that the total moment transmitted to the foundation is mostly balanced by the push-pull moment, apparently a

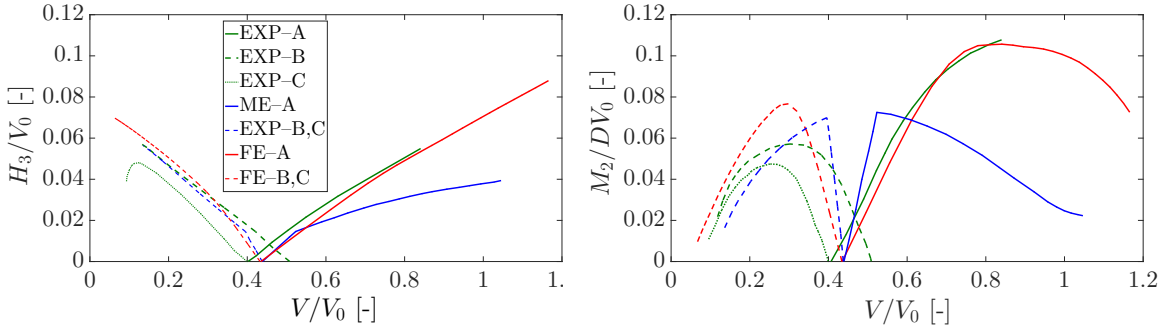

(a) horizontal-vertical ($H_3/V_0 - V/V_0$) (b) moment-vertical ($M_2/DV_0 - V/V_0$)

Figure 9: Spudcan load paths during symmetric pushover – *Note*: all experimental measurements on spudcan A terminated earlier than for spudcans B-C due exceeded bending gauge capacity (Bienen et al., 2009).

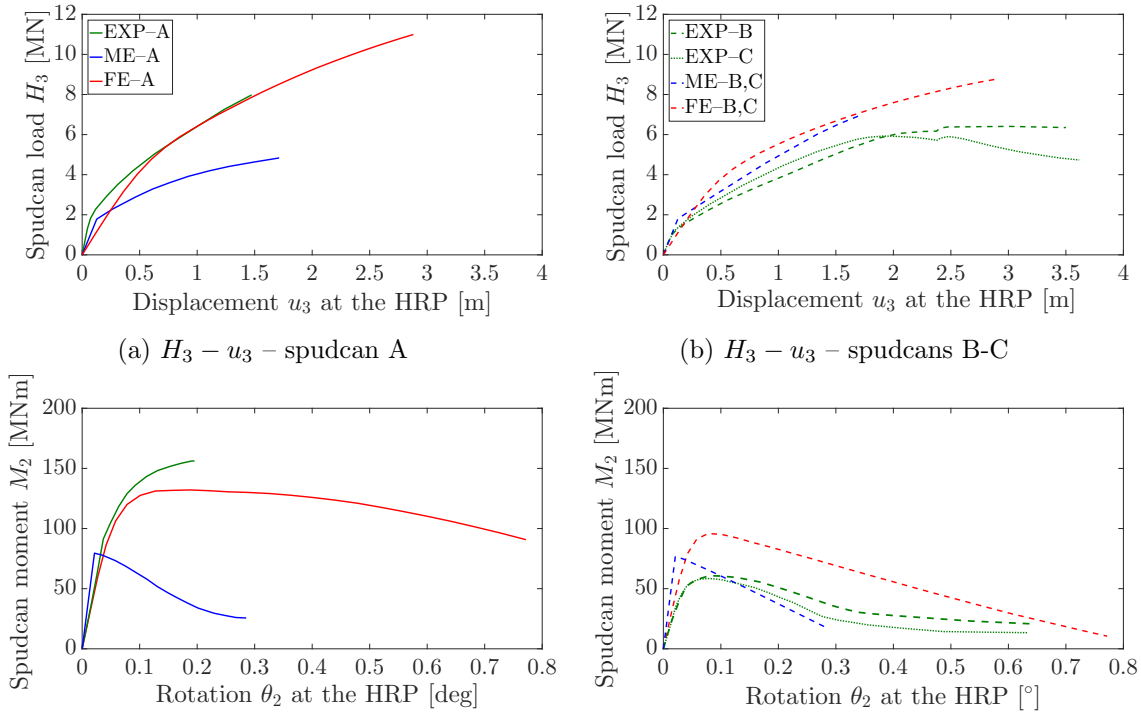

(a) $H_3 - u_3$ – spudcan A (b) $H_3 - u_3$ – spudcans B-C

(c) $M_2 - \theta_2$ – spudcan A (d) $M_2 - \theta_2$ – spudcans B-C

Figure 10: Spudcan force-displacement and moment-rotation responses during symmetric pushover – *Note*: all experimental measurements on spudcan A terminated earlier than for spudcans B-C due exceeded bending gauge capacity (Bienen et al., 2009).

stiffer load-attractor than individual spudcan fixities. Nonetheless, the vanishing of local moments at the windward spudcans (see Figure 10d[8]) disrupts the load redistribution occurring during lateral pushover and correctly captured by ME and FE results (Figures 10c–10d). In other words, the jack-up unit fails due to the push-pull moment at the foundation not compensating for the vanishing spudcan moments.

[8]the FE M_2 moment is "almost" nil as the numerical results have been plotted up to the last fully converged step.

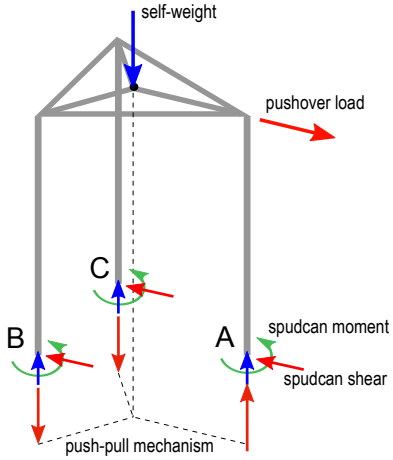

(a) equilibrium diagram

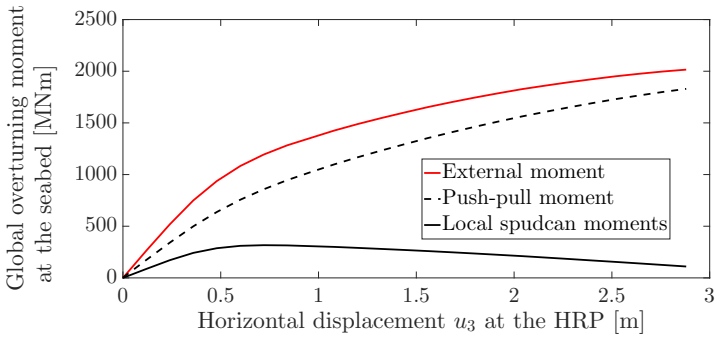

(b) push-pull vs local spudcan moments from 3D FE analysis

Figure 11: Evolution of moment-resisting mechanisms during symmetric pushover.

4.2 Misaligned lateral pushover – $\omega = 22°$

The validation of the continuum FE model is taken further by considering the misaligned pushover depicted in Figure 6. As the horizontal load is applied with a deviation of 22° from the symmetry axis of the hull, the jack-up topside undergoes a combination of horizontal and torsional loading. As a consequence, the three spudcans experience real six degrees-of-freedom loading, including horizontal-moment components along both axes 2 and 3 and torsion (Bienen and Cassidy, 2006; Bienen et al., 2006). Unfortunately, spudcan torques were not measured during the reference centrifuge tests, although duly considered in the corresponding ME-based simulations (Bienen et al., 2009).

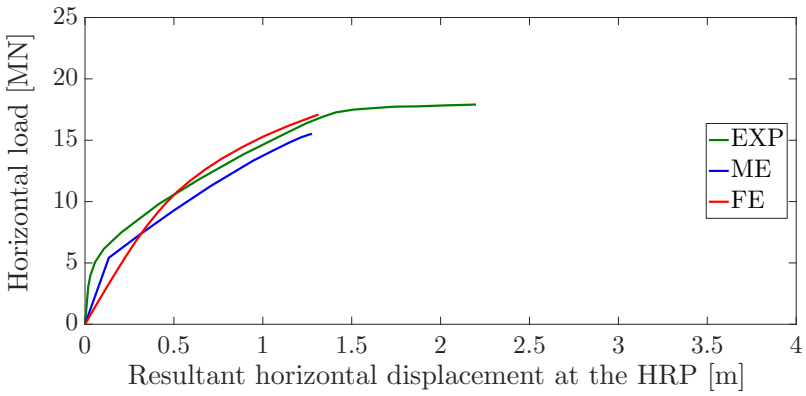

Figure 12: Jack-up response to misaligned pushover – comparison among EXP, ME and FE results.

Figures 12 to 14 repropose for the case of misaligned pushover the same EXP-ME-FE comparison. Regarding the global load-displacement response at the hull, Figure 12 supports conclusions similar to those drawn for symmetric pushover (Figure 7a): as explained in Section 4.1, the continuum FE model predicts less accurately the initial stiffness emerging from centrifuge tests, but with an even better match of the ultimate capacity (EXP: 17.9 MN; FE: 17.1 MN; ME: 15.5 MN). It is worth noting that FE and ME load-displacement curves attain failure at similar values of (resultant) lateral displacement, although quite lower than the experimental value. Also in this case, the FE response at the HRP does not fully attain a flat plateau, due to FE results being available up to the last

converged calculation step.

The FE predictions of the horizontal-moment load paths along axis 3 (Figure 13a) and axis 2 (Figure 13b) are mostly closer to EXP measurements than ME results, especially for spudcan A along axis 3. Similar inferences are also supported by the horizontal load-displacement response displayed in Figure 14, again concerning all spudcans and both horizontal directions. As pointed out in Section 3.2.2, the discrepancies between EXP and ME/FE results do not necessarily come from inaccurate numerical modelling, but also from experimental imperfections and lacking data for model calibration – in this respect the uneven penetration/preloading achieved by the three spudcans in the centrifuge should be recalled.

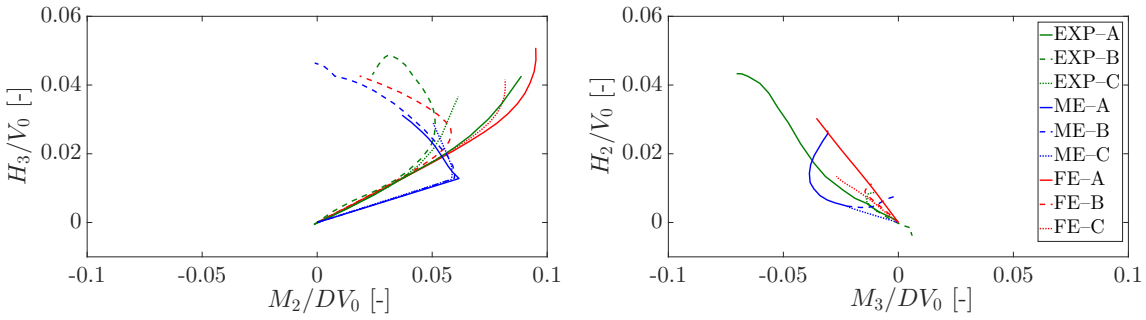

(a) horizontal-moment 1 ($H_3/V_0 - M_2/DV_0$) (b) horizontal-moment 2 ($H_2/V_0 - M_3/DV_0$)

Figure 13: Spudcan load paths during misaligned pushover.

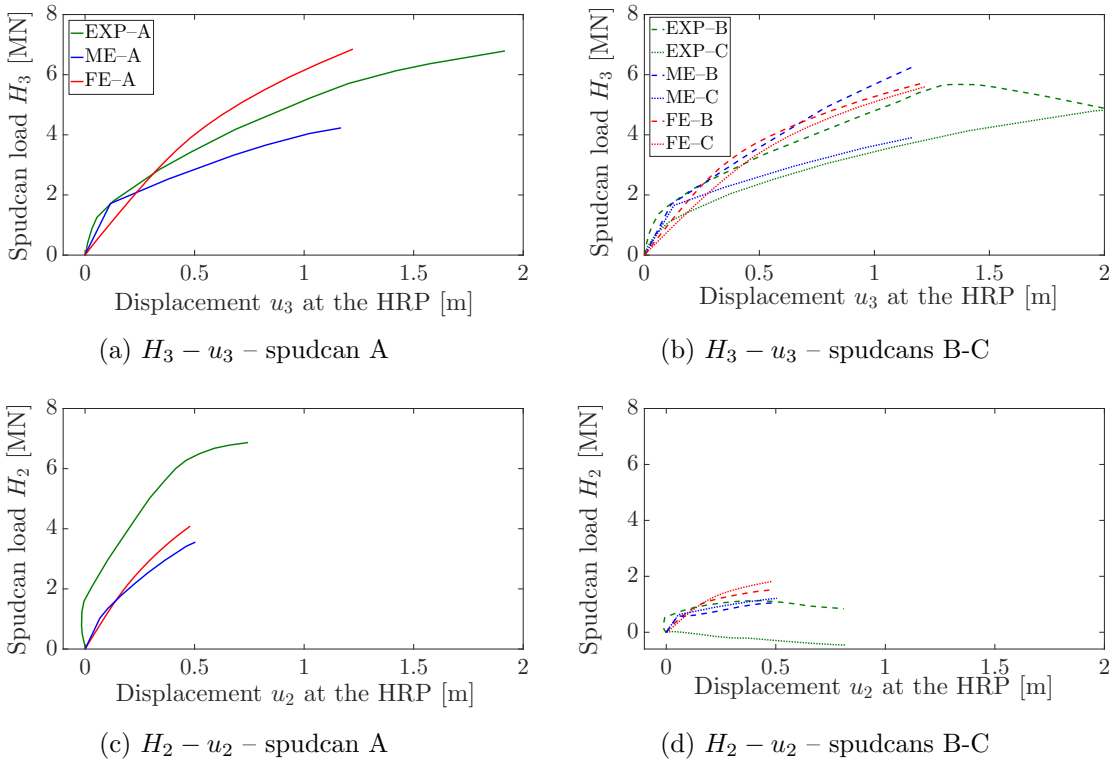

(a) $H_3 - u_3$ – spudcan A (b) $H_3 - u_3$ – spudcans B-C

(c) $H_2 - u_2$ – spudcan A (d) $H_2 - u_2$ – spudcans B-C

Figure 14: Spudcan force-displacement responses during misaligned pushover.

While the goal of this validation section is to unveil the predictive potential of fully 3D simulations,

readers may refer to (Bienen et al., 2009) for deeper physical insight into the mechanics of jack-up–spudcan-soil interaction under misaligned pushover. The EXP-ME-FE cross-comparison for general 3D loading supports the conclusion that continuum simulations can provide results as accurate as, and possibly better than, ME-based predictions. The computational extra-costs of continuum modelling may be worth bearing to foster the development of lumped (ME) interaction models for engineering applications.

5 Insight from parametric studies

The above validation tests give confidence about the accuracy and robustness of the continuum 3D FE model. The predictive potential of the same jack-up model is further explored in this section. This will promote the use of 3D FE modelling to learn more lessons about the mechanics of jack-up–soil systems, and in turn support the development of simplified approaches – such as ME models.

5.1 Influence of soil modelling assumptions

The use of more advanced soil constitutive models may be hindered by the lack of comprehensive soil data for parameter calibration (see Section 3.2.2). In this respect, it is instructive to perform a numerical experiment in which the consequences of "poorer" soil modelling are investigated. Such an experiment aims to point out non-intuitive effects of soil modelling assumptions on the response of jack-ups. It should be remarked that soil constitutive models have been traditionally developed for civil engineering applications, so there is less knowledge available in relation to peculiar marine structures like jack-ups.

Figures 15a–15b displays how the MMC model as formulated/calibrated above (Figure 4) has been degraded in two steps:

- "MMC–1": first, the shear hardening has been inhibited while keeping the same oedometric compression behaviour (i.e. cap hardening unaltered). This has been achieved by setting $\phi_0 = \phi_f$ in Equation (5), as well as a lower K_{ref} in Equation (2) to approximate the variable MMC deviatoric stiffness with a constant secant value;

- "MMC–2": cap hardening has then been prevented by setting high initial values of the p_c hardening variable in the soil domain (Equation (3)), along with $n = 1$ in Equation (2) to remove elastic non-linearity. As visible in Figure 15b, this results in constant oedometric stiffness, not capturing soil stiffening at increasing compressive stress. In this case, the elastic shear stiffness has been set equal to the higher MMC small-strain value (Figure 15a).

Figure 15c shows that loosing accuracy on triaxial/deviatoric soil behaviour affects negligibly the global performance of the jack-up, as long as the pre-failure shear stiffness is given a sound secant value – even if constant. Conversely, remarkable losses in jack-up stiffness/capacity result from inhibiting the MMC cap mechanism and the locking/pressure-dependent behaviour of the sand under oedometer compression (MMC–2 case). This seems closely related to the plots in Figure 11b: since the external moment is mostly resisted through spudcan push-pulling, modelling the soil response to confined compression (i.e. nearly oedometric) proves more influential than triaxial conditions (usually of the most concern in constitutive modelling research). Figure 16 complements this analysis by displaying the local loading paths, $H_3 - V$ and $M_2 - V$, experienced by all spudcans in relation to MMC, MMC-1 and MMC-2 sand modelling. While Figure 16a shows the low influence of such constitutive assumptions on the mobilised foundation shear, Figure 16b illustrates that also local spudcan moments – not only global push-pulling – can be significantly affected by the inaccurate modelling of soil compression (compare to Figure 15b). In particular, not capturing soil locking under

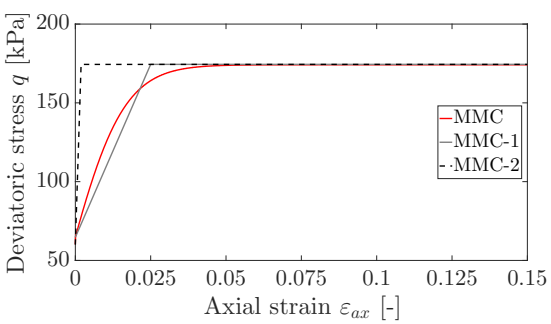

(a) comparison among triaxial performances

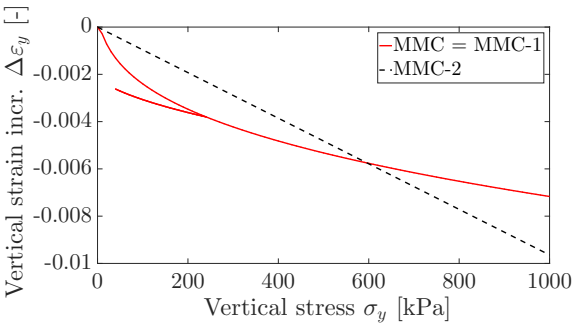

(b) comparison among oedometric performances

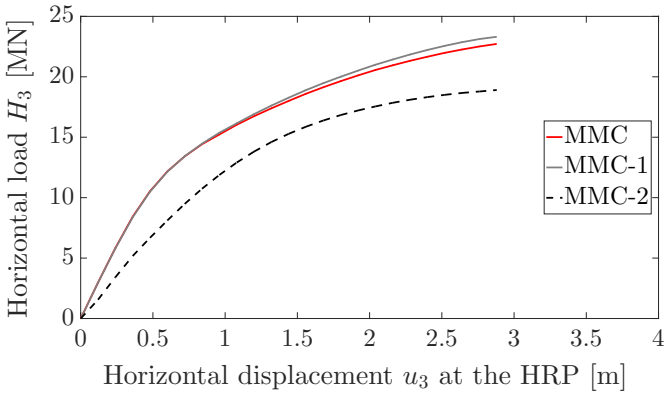

(c) comparison among global force-displacement responses at the hull.

Figure 15: Influence of soil modelling assumptions on the jack-up response to lateral pushover.

mixed settlement/rotation leads to an obvious reduction of local moment components, still relevant contributors to the pushover response of the jack-up (see Figure 11b).

The above observations help clarify what prerequisites soil constitutive relationships should meet for reliable 3D jack-up analyses. This topic will deserve further discussion in relation to cyclic/dynamic loading conditions and the use of soil models featuring kinematic shear hardening. The latter is not only essential to capture the cyclic hysteresis of soils, but also expected to affect stress conditions around all spudcans prior to lateral loading, i.e. after pre-loading and unloading.

5.2 Additional 3D pushover analyses

The FE model as validated in Section 4 is used here to explore the response to different 3D loading combinations, namely a misaligned lateral pushover with $\omega = 60°$ (load applied at the HRP) and a pure torsional pushover (Figure 17).

5.2.1 Misaligned lateral pushover – $\omega = 60°$

The load orientation $\omega = 60°$ is such that legs A and C work as leeward, while spudcan B will experience decreasing compression during lateral pushover. Since the hull is not exactly equilateral, the combined loading paths undergone by spudcans A and C are anticipated to differ slightly – expectation confirmed by the 3D FE results. This new case and the previous two are all lateral pushovers, although with the following differences:

1. $\omega = 0°$ – symmetric pushover along axis 3, windward legs B-C (identical in the model) and leeward leg A;

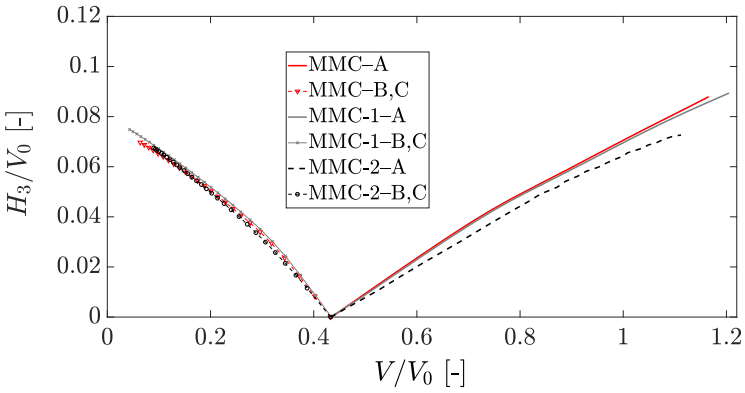

(a) horizontal-vertical ($H_3/V_0 - V/V_0$)

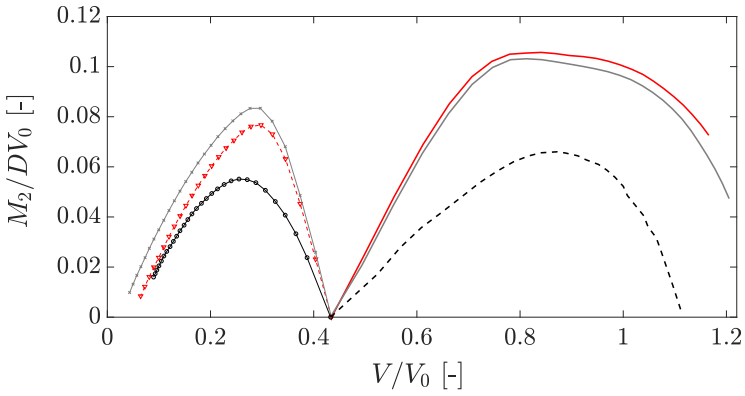

(b) moment-vertical ($M_2/DV_0 - V/V_0$)

Figure 16: Influence on soil modelling assumption on spudcan load paths during symmetric pushover.

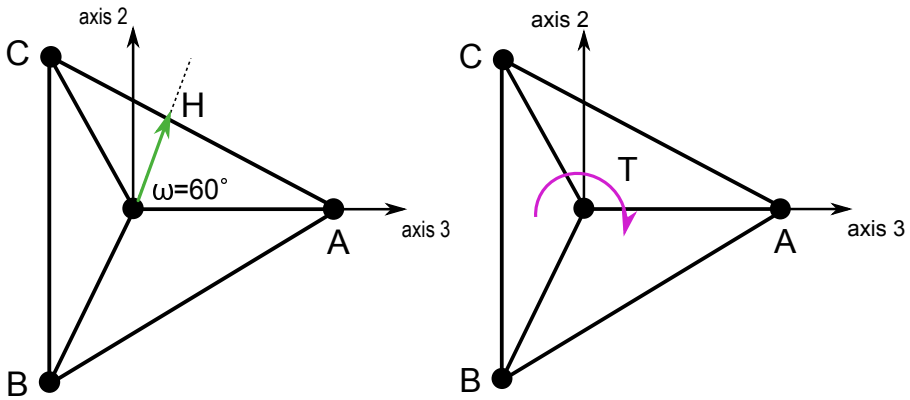

(a) lateral pushover – $\omega = 60°$ (b) torsional pushover

Figure 17: Loading conditions for additional pushover analyses.

2. $\omega = 22°$ – misaligned pushover with eccentric load application at the vertex A of the hull (as in Bienen et al.'s physical model). The hull is thus subjected to horizontal-torsional loading. All spudcans undergo different loading paths, with the jack-up "pivoting around spudcan C while tilting in the direction of the pull"(Bienen et al., 2009). Spudcan B is the footing lifting off at

the onset of failure;

3. $\omega = 60°$ – misaligned pushover with no torque with respect to the HRP. B is the only pure windward leg.

In Figure 18 the structural performances for $\omega = 0°, 22°, 60°$ are compared in terms of global load-displacement response (Figure 18a, total resultant horizontal displacement considered for misaligned cases) and horizontal-moment $H_3 - M_2$ load paths for spudcans A and B (Figure 18b, note that $H_2 - M_3$ paths are nil for $\omega = 0°$ due to symmetry). Figure 18a confirms clearly the dependence of the ultimate jack-up capacity on the load orientation, as a consequence of different resisting mechanisms developed by the whole tripodal foundation. As expected, relying on one ($\omega = 22°, 60°$) or two ($\omega = 0°$) uplifting legs can affect drastically such capacity, with the uplift-moment failure of the windward spudcan occurring earlier when acting individually. Further insight about this aspect can be gained from the $H_3/V_0 - M_2/DV_0$ load paths in Figure 18b : the compression force on spudcan B exhibits the fastest reduction for $\omega = 60°$, which in turns determines the sharpest drop in moment M_2 and the lowest mobilisation of foundation shear H_3.

It is also interesting to notice that, unlike the ultimate capacity, the global lateral stiffness seems negligibly affected by load orientation, even in presence of a parasitic torque (see $\omega = 22°$ case). The redundant structure founded on the (elasto-plastic) soil can redistribute over the three legs the variations in axial force, in a way that preserves a unique lateral stiffness.

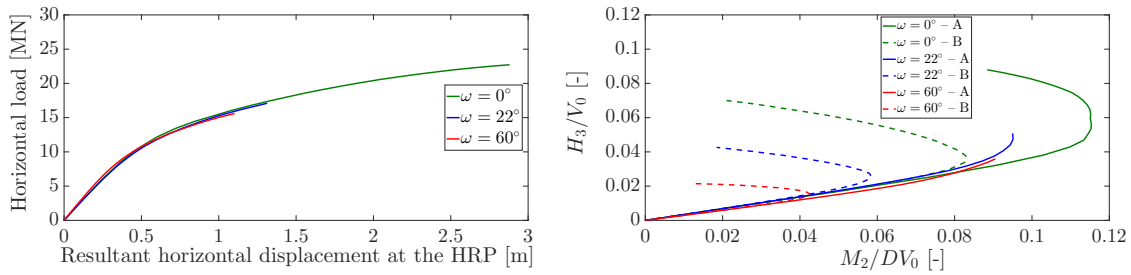

(a) horizontal force-displacement response at the hull

(b) horizontal-moment spudcan load paths ($H_3/V_0 - M_2/DV_0$)

Figure 18: Comparison among the responses to symmetric ($\omega = 0°$) and misaligned ($\omega = 22°, 60°$) pushover.

5.2.2 Torsional pushover

The response to pure hull torsion is examined as an ideal loading scenario (Figure 17b), whereas torsion is normally induced in reality by misaligned lateral loading – the simulation of the latter case has been already discussed in Section 4.2 to validate the model with respect to "realistic" horizontal-torsional loading. Current state of practice only accounts for planar soil-spudcan interaction, 2D VHM loading (ISO, 2016), even though relevant interactions among all six degrees-of-freedom have been already put in evidence for fully 3D (non-symmetric) loading (Bienen and Cassidy, 2006). To date, only very few experimental and numerical works have explored the consequences of spudcan torsion (Bienen et al., 2006, 2007; Salciarini and Tamagnini, 2009; Tamagnini et al., 2013), so that ample room seems still to be there for further studies in the area. The potential of 3D FE modelling to also capture the interaction between global and local torsion is discussed hereafter with regard to the loading case in Figure 17b – pure torque applied at the hull, positive according to orientation of axis 1 in Figure 3a.

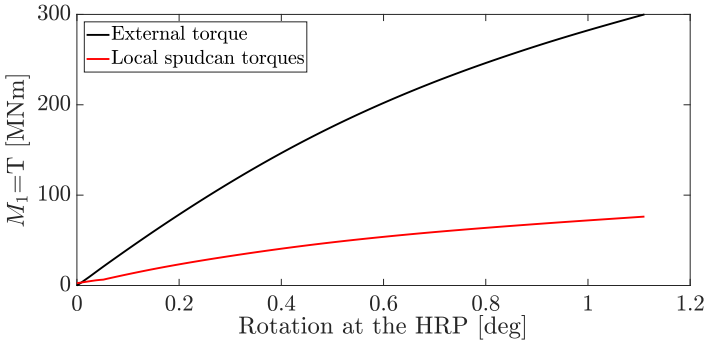

(a) torque-twist response at the hull and quota from the sum of single spudcan torques

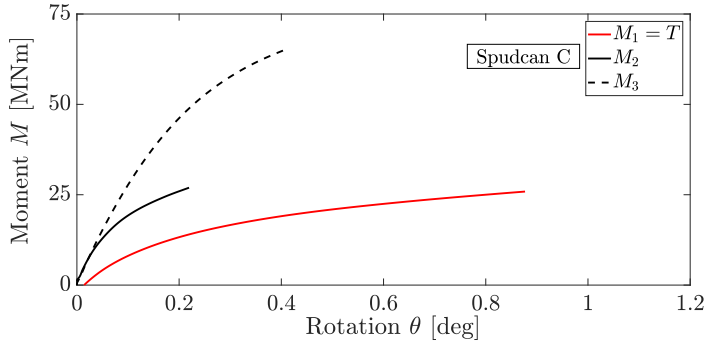

(b) moment-rotation responses ($M_1/DV_0 - \theta_1$, $M_2/DV_0 - \theta_2$, $M_3/DV_0 - \theta_3$) at spudcan C

Figure 19: Jack-up response to torsional pushover.

In a large deformation framework, jack-ups resist torsion at the foundation through two mechanisms: one arises from local torques at each spudcan, the second from spudcan shear forces that are eccentric with respect to the HRP. Although the second mechanism is commonly deemed dominant, Figure 19a shows that a non-negligible quota of the external torque may actually be resisted by the sum of spudcan torques (in this case approximately 25% of the total). In this case a 1°-rotation of the hull is associated with a total torque of about 300 MNm, approximately four times the value associated with the misaligned horizontal load considered in Section 4.2. Prominent global torsion and significant spudcan torques may be promoted by alternative hull geometries (see e.g. the elongated shape in Figure 1b) and/or high(er) torsional stiffness of the legs.

For further inspection, Figure 19b illustrates the three moment-rotation curves recorded at spudcan C during torsional pushover – the signs of spudcan moments/rotations are consistent with the axes orientations in Figure 3a. The curves in Figure 19b shows that the torque recorded at the spducan-leg connection is quantitatively comparable to the other "bending" moments, as well as that all rotation components share comparable orders of magnitude. In particular, the maximum torque experienced by spudcan C is a non-negligible fraction of its (after-preloading) torsional capacity, found numerically equal to 76.2 MNm. These results stress once more the relevance of including all six degrees-of-freedom in macroelement approaches: according to these FE results, simplifying assumptions such as infinite or nil torsional stiffness may cause significant inaccuracies.

6 Concluding remarks

A fully 3D FE model based on continuum soil plasticity was set up for the operational analysis of jack-ups. In particular, the Modified Mohr-Coulomb strain-hardening model was selected and calibrated for a dense sandy subgrade, along with a Total Lagrangian problem formulation able to capture large deformation ($P - \Delta$) effects – quantitatively very relevant in flexible structures such as jack-ups.

The performance of the FE model under static/monotonic pushover was successfully validated for a mid-size three-legged jack-up against previous centrifuge test results and macroelement-based simulations. The FE model could reproduce not only the global behaviour of the jack-up–spudcans–soil system, but also local load paths and displacements/rotations at each spudcan. The 3D FE model was then used to highlight certain implications of soil modelling assumptions, as well as to discuss the structural response to other 3D loading scenarios:

- the level of complexity of the MMC formulation appeared necessary to correctly simulate the structural behaviour emerging from centrifuge tests. Simpler soil modelling resulted in inaccurate foundation mechanisms (spudcan push-pull). Preserving accuracy on the simulation of confined soil compression (oedometric) proved essential, as long as enough laboratory data are available to calibrate relevant soil parameters;

- the FE model could capture the expected influence of load orientation on the global failure mechanism of the structure. In particular, varying orientations of the horizontal push-over load gave rise to different realisation of foundation push-pull, and in turn determined different ultimate limit loads;

- the analysis of pure torsional pushover pointed out that local spudcan torsion/twist can contribute significantly to the global torque-resisting mechanism. This confirmed the importance of modelling jack-up–spudcans–soil interaction beyond the most common planar/symmetric schemes used in practice.

Accurate continuum FE models are not only a value per se, but should also be reappraised to keep improving lumped macroelement models. Currently, macroelements are mostly formulated and calibrated based on small scale experiments, only rarely accounting for all six degrees-of-freedom. Well-validated 3D FE models could limit the need for demanding experimental programmes, and complement the evidence from existing data set. At the same time, FE modelling is intrinsically suitable for extension to loading conditions more complex than what considered here, involving e.g. partial pore water drainage, cyclic loading and/or dynamic effects. These cases still challenge the use of existing macroelement formulations, valuable input to their improvement could come from continuum two-phase FE simulations with advanced cyclic soil models (Corciulo et al., 2017).

Acknowledgements

Robbin Schipper thanks DIANA FEA for hosting his MSc graduation project. All authors warmly acknowledge Cristina Jommi (Politecnico di Milano/TU Delft) for contributing to the discussion about this work, and Hugo Hofstede (GustoMSC) for kindly providing the pictures in Figures 1a–1b. The feedback of three anonymous reviewers is also highly appreciated.

References

Andresen, L., Jostad, P. H., and Andersen, K. H. (2010). Finite element analyses applied in design of foundations and anchors for offshore structures. *International Journal of Geomechanics*, 11(6):417–430.

Bathe, K.-J. (1982). Finite element procedures in engineering analysis.

Bienen, B., Byrne, B., Houlsby, G., and Cassidy, M. (2006). Investigating six-degree-of-freedom loading of shallow foundations on sand. *Géotechnique*, 56(6):367–380.

Bienen, B. and Cassidy, M. (2006). Advances in the three-dimensional fluid–structure–soil interaction analysis of offshore jack-up structures. *Marine Structures*, 19(2):110–140.

Bienen, B. and Cassidy, M. (2009). Three-dimensional numerical analysis of centrifuge experiments on a model jack-up drilling rig on sand. *Canadian Geotechnical Journal*, 46(2):208–224.

Bienen, B., Cassidy, M., and Gaudin, C. (2009). Physical modelling of the push-over capacity of a jack-up structure on sand in a geotechnical centrifuge. *Canadian Geotechnical Journal*, 46(2):190–207.

Bienen, B., Gaudin, C., and Cassidy, M. (2007). Centrifuge tests of shallow footing behaviour on sand under combined vertical-torsional loading. *International Journal of Physical Modelling in Geotechnics*, 7(2):01–21.

Cassidy, M., Martin, C., and Houlsby, G. (2004). Development and application of force resultant models describing jack-up foundation behaviour. *Marine Structures*, 17(3):165–193.

Cassidy, M., Taylor, P., Taylor, R. E., and Houlsby, G. (2002). Evaluation of long-term extreme response statistics of jack-up platforms. *Ocean engineering*, 29(13):1603–1631.

Cassidy, M., Taylor, R. E., and Houlsby, G. (2001). Analysis of jack-up units using a constrained NewWave methodology. *Applied Ocean Research*, 23(4):221–234.

Cassidy, M. J., Vlahos, G., and Hodder, M. (2010). Assessing appropriate stiffness levels for spudcan foundations on dense sand. *Marine Structures*, 23(2):187–208.

Cheng, N. (2015). *Force-resultant models for shallow foundation systems and their implementation in the analysis of soil-structure interactions*. PhD thesis, University of Western Australia.

Cheong, J. (2002). Physical testing of jack-up footings on sand subjected to torsion. B.E. Honours thesis. University of Western Australia.

Corciulo, S., Zanoli, O., and Pisanò, F. (2017). Transient response of offshore wind turbines on monopiles in sand: role of cyclic hydro–mechanical soil behaviour. *Computers and Geotechnics*, 83:221–238.

Dafalias, Y. F. and Manzari, M. T. (2004). Simple plasticity sand model accounting for fabric change effects. *Journal of Engineering mechanics*, 130(6):622–634.

De Borst, R., Sluys, L., Muhlhaus, H.-B., and Pamin, J. (1993). Fundamental issues in finite element analyses of localization of deformation. *Engineering computations*, 10(2):99–121.

Dean, E., Hsu, Y., James, R., Sasakura, T., Schofield, A., and Tsukamoto, Y. (1997a). Centrifuge modelling of jackups and spudcans on drained and partially drained silica sand. *Marine Structures*, 10(2-4):221–241.

Dean, E., James, R., Schofield, A., and Tsukamoto, Y. (1998). Drum centrifuge study of three-leg jackup models on clay. *Géotechnique*, 48(6):761–786.

Dean, E., James, R., Schofield, A. N., and Tsukamoto, Y. (1997b). Numerical modelling of three-leg jackup behaviour subject to horizontal load. *Soils and Foundations*, 37(2):17–26.

di Prisco, C. and Pisanò, F. (2011). Seismic response of rigid shallow footings. *European Journal of Environmental and Civil Engineering*, 15(sup1):185–221.

Elgamal, A., Yang, Z., Parra, E., and Ragheb, A. (2003). Modeling of cyclic mobility in saturated cohesionless soils. *International Journal of Plasticity*, 19(6):883–905.

Georgiadis, M. and Butterfield, R. (1988). Displacements of footings on sand under eccentric and inclined loads. *Canadian Geotechnical Journal*, 25(2):199–212.

Goodman, R. E., Taylor, R. L., and Brekke, T. L. (1968). A model for the mechanics of jointed rock. *Journal of the Soil Mechanics and Foundations Division*, 94(3):637–660.

Gottardi, G., Houlsby, G., and Butterfield, R. (1999). Plastic response of circular footings on sand under general planar loading. *Géotechnique*, 49(4):453–470.

Groen, A. E. (1997). *Three-dimensional elasto-plastic analysis of soils*. PhD thesis, Delft University of Technology.

Holzapfel, G. A. (2000). *Nonlinear Solid Mechanics: A Continuum Approach for Engineering*. John Wiley & Sons.

Houlsby, G. (2016). Interactions in offshore foundation design. *Géotechnique*, 66(10):791–825.

Houlsby, G., Abadie, C., Beuckelaers, W., and Byrne, B. (2017). A model for nonlinear hysteretic and ratcheting behaviour. *International Journal of Solids and Structures*, 120:67–80.

Houlsby, G. and Cassidy, M. (2002). A plasticity model for the behaviour of footings on sand under combined loading. *Géotechnique*, 52(2):117–129.

Hoyle, M., Stiff, J., Hunt, R., Morandi, A., et al. (2006). Jack-up assessment - past, present and ISO. In *The Sixteenth International Offshore and Polar Engineering Conference*. International Society of Offshore and Polar Engineers.

ISO (2016). ISO 19905-1 petroleum and natural gas industries - Site-specific assessment of mobile offshore units - Part 1: Jack-ups. Technical report, International Organization for Standardization.

Karunakaran, D., Bærheim, M., and Spidsøe, N. (1999). Full-scale measurements from a large deepwater jack-up platform. *Marine Structures*, 12(4):255–275.

Kellezi, L., Denver, H., Kudsk, G., and Stadsgaard, H. (2007). FE skirted footings analyses for combined loads and layered soil profile. In *Proceedings of 14th European Conference on Soil Mechanics and Geotechnical Engineering*, pages 341–346.

Kellezi, L., Kudsk, G., and Hofstede, H. (2008). Jack-up rig foundation design applying 3D FE structure-soil-interaction modeling. In *Proceedings of the BGA International Conference on Foundations*, pages 24–27.

Kementzetzidis, E., Versteijlen, W. G., Nernheim, A., and Pisanò, F. (2018). 3d fe dynamic modelling of offshore wind turbines in sand: natural frequency evolution in the pre–to after-storm transition. In *Numerical Methods in Geotechnical Engineering IX, Volume 1: Proceedings of the 9th European Conference on Numerical Methods in Geotechnical Engineering (NUMGE 2018), June 25-27, 2018, Porto, Portugal*, pages 1477–1484. CRC Press.

Liu, H., Zygounas, F., Diambra, A., and Pisano, F. (2018). Enhanced plasticity modelling of high-cyclic ratcheting and pore pressure accumulation in sands. In *Numerical Methods in Geotechnical Engineering IX, Volume 1: Proceedings of the 9th European Conference on Numerical Methods in Geotechnical Engineering (NUMGE 2018), June 25-27, 2018, Porto, Portugal*, page 87. CRC Press.

Manie, J. (2016). DIANA FEA BV. User's Manual - release 10.1. Technical report, DIANA FEA BV.

Martin, C. and Houlsby, G. (2001). Combined loading of spudcan foundations on clay: numerical modelling. *Géotechnique*, 51(8):687–700.

Nelson, K., Smith, P., Hoyle, M., Stonor, R., Versavel, T., et al. (2000). Jack-up response measurements and the underprediction of spud-can fixity by SNAME 5-5A. In *Offshore Technology Conference*. Offshore Technology Conference.

Niemunis, A. and Herle, I. (1997). Hypoplastic model for cohesionless soils with elastic strain range. *Mechanics of Cohesive-frictional Materials*, 2(4):279–299.

Nova, R. (2012). *Soil mechanics*. John Wiley & Sons.

Nova, R. and Montrasio, L. (1991). Settlements of shallow foundations on sand. *Géotechnique*, 41(2):243–256.

Osborne, J., Houlsby, G., Teh, K., Bienen, B., Cassidy, M., Randolph, M., and Leung, C. (2009). Improved guidelines for the prediction of geotechnical performance of spudcan foundations during installation and removal of jack-up units. In *Proceedings of the 41st Offshore Technology Conference, Houston, OTC*, volume 20291.

Pisanò, F., di Prisco, C., and Lancellotta, R. (2014). Soil-foundation modelling in laterally loaded historical towers. *Géotechnique*, 64(1):1.

Pucker, T., Bienen, B., and Henke, S. (2013). CPT based prediction of foundation penetration in siliceous sand. *Applied Ocean Research*, 41:9–18.

Purwana, O. A., Perry, M. J., Quah, M., Cassidy, M. J., et al. (2012). Comparison of ISO 19905-1 framework and a plasticity-based spudcan model for jackup foundation assessments. In *Offshore Technology Conference*. Offshore Technology Conference.

Ragni, R., Wang, D., Mašín, D., Bienen, B., Cassidy, M. J., and Stanier, S. A. (2016). Numerical modelling of the effects of consolidation on jack-up spudcan penetration. *Computers and Geotechnics*, 78:25–37.

Randolph, M. and Gourvenec, S. (2011). *Offshore geotechnical engineering*. CRC Press.

Rowe, P. W. (1962). The stress-dilatancy relation for static equilibrium of an assembly of particles in contact. In *Proceedings of the Royal Society of London A: Mathematical, Physical and Engineering Sciences*, volume 269, pages 500–527. The Royal Society.

Salciarini, D. and Tamagnini, C. (2009). A hypoplastic macroelement model for shallow foundations under monotonic and cyclic loads. *Acta Geotechnica*, 4(3):163–176.

Schotman, G. (1989). The effects of displacements on the stability of jackup spudcan foundations. In *Offshore Technology Conference*. Offshore Technology Conference.

Schotman, G. and Efthymiou, M. (1989). Aspects of the stability of jack-up spud-can foundations. *Marine Structures*, 2(3-5):425–449.

Simo, J. and Hughes, T. (1998). *Computational inelasticity*. Springer.

SNAME (2008). Guidelines for site specific assessment of mobile jack-up units. Technical and Research bulletin 5-5A Rev. 3, Society of Naval Architechts and Marine Engineers.

Svanø, G. and Tjelta, T. I. (1996). Skirted spud-cans—extending operational depth and improving performance. *Marine Structures*, 9(1):129–148.

Tamagnini, C., Salciarini, D., and Ragni, R. (2013). Implementation of 6–dof hypoplastic macroelement in a finite element code. In *Proceedings of third international symposium on computational geomechanics (ComGeo III). Berlin: Springer*.

Vlahos, G., Cassidy, M., and Martin, C. (2011). Numerical simulation of pushover tests on a model jack-up platform on clay. *Geotechnique*, 61(11):947–960.

Vlahos, G., Cassidy, M. J., and Byrne, B. W. (2006). The behaviour of spudcan footings on clay subjected to combined cyclic loading. *Applied Ocean Research*, 28(3):209–221.

Vlahos, G., Cassidy, M. J., and Martin, C. M. (2008). Experimental investigation of the system behaviour of a model three-legged jack-up on clay. *Applied Ocean Research*, 30(4):323–337.

Vlahos, G., Martin, C. M., Prior, M. S., and Cassidy, M. J. (2005). Development of a model jack-up unit for the study of soil-structure interaction on clay. *International Journal of Physical Modelling in Geotechnics*, 5(2):31–48.

Wong, P. C., Templeton III, J., Purwana, O. A., Hofstede, H., Cassidy, M. J., Hossain, M. S., Martin, C., et al. (2012). Foundation modeling and assessment in the new ISO standard 19905-1. In *Offshore Technology Conference*. Offshore Technology Conference.

Zhang, Y., Bienen, B., and Cassidy, M. J. (2014a). Jack-up push-over analyses featuring a new force resultant model for spudcans in soft clay. *Ocean Engineering*, 81:139–149.

Zhang, Y., Cassidy, M. J., and Bienen, B. (2014b). A plasticity model for spudcan foundations in soft clay. *Canadian Geotechnical Journal*, 51(6):629–646.

A Sensitivity of lateral pushover results to FE discretisation

A relevant aspect of FE analyses is the set-up of a suitable FE mesh, so as to achieve an acceptable trade-off between accuracy (convergence to solution) and computational costs. As mentioned in Section 3.4, the latter demands special attention in the case of strongly non-linear 3D simulations. Figure 20a illustrates how the soil domain was partitioned prior to FE meshing with tetra/hexa-elements. Table 3 reports the average element size within each size zone (A, B, C, D) for the three meshes considered (1–coarse, 2–intermediate, 3–fine). Obviously, smaller element size have been set close to the three spudcans, in order to accurately reproduce sharper stress gradients and plastic straining – see Figure 20b.

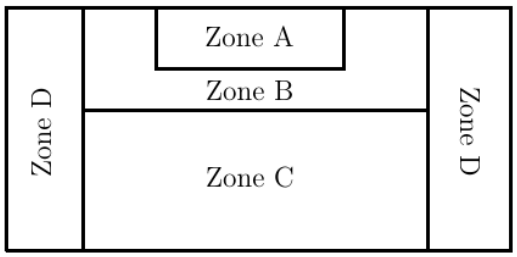

(a) 3D model domain partition

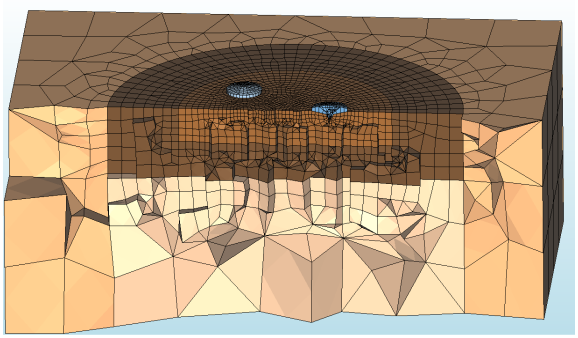

(b) mesh 2 (Table 3) – vertical cross-section

Figure 20: Non-uniform FE size within the 3D model domain.

Figure 21 reports the performance of the three meshes with reference to the same symmetric lateral pushover discussed in Secton 4.1. The results in the figure led to prefer the "intermediate" mesh 2 over the finer mesh 3, with the former reducing substantially the computational burden: only minimal differences in the predicted pushover curves are observed, which seems acceptable in light of the demonstrative character of this work.

Table 3: Mesh sensitivity study – FE size distribution within the 3D model domain.

Mesh	FE size [m] – spudcan	FE size [m] – soil (Figure 20a)			
		Zone A	Zone B	Zone C	Zone D
mesh 1 – coarse	2	4	8	20	20
mesh 2 – intermediate	1	2	4	15	20
mesh 3 – fine	1	1.5	2	15	20

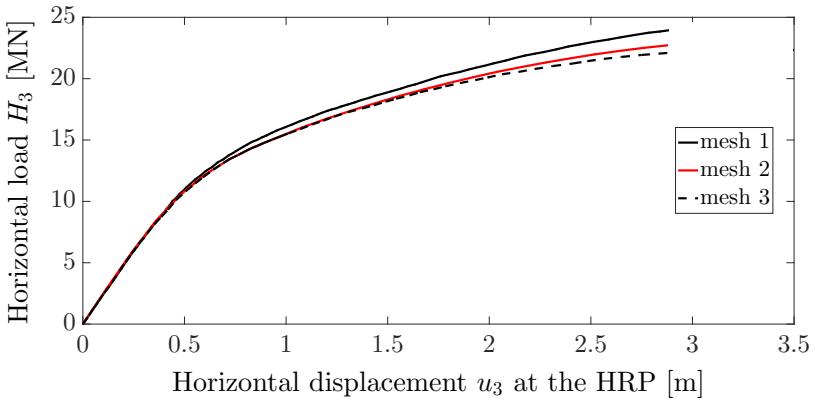

Figure 21: Jack-up performance under symmetric lateral pushover at varying FE discretisation – horizontal force-displacement response at the hull (Section 4.1).

The overall accuracy achieved with a given mesh is also affected by the convergence criteria set for the global Newton-Raphson iterations. In particular, the calculation stages associated with static pushover have been performed by aiming to fulfil at the same time two distinct accuracy criteria:

$$\text{Relative Force Error} = \frac{\sqrt{g_i^T g_i}}{\sqrt{g_0^T g_0}} \leq 10^{-3}, \quad \text{Relative Displacement Error} = \frac{\sqrt{\Delta u_i^T \Delta u_i}}{\sqrt{\Delta u_i^T \Delta u_i}} \leq 10^{-3} \quad (9)$$

where $\mathbf{g}$ is the vector of out-of-balance forces and $\mathbf{\Delta u}$ the incremental displacement in each step increment; subscripts i and 0 denote the i^{th} and the first iterations in a given calculation step. Although tighter convergence criteria are often recommended, it would be hard in practice to finalise such non-linear FE calculations under harsher requirements.

B Vertical load-settlement response of a single spudcan

This appendix gives some insight into the vertical load-settlement response of single spudcans in the 3D FE model, as a relevant contributor to the lateral pushover behaviour of the jack-up. In particular, possible motivations for the difference in global initial stiffness between EXP and FE results (see Figure 7a in Section 4.1) are discussed in more detail.

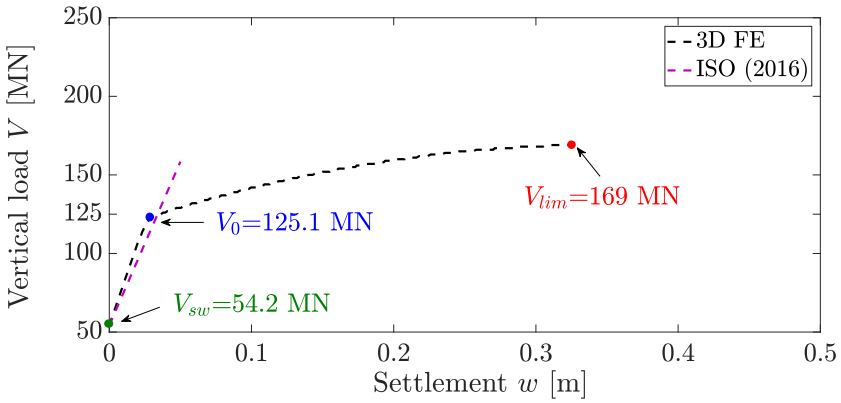

Figure 22: Simulated load-settlement response of a single spudcan.

Figure 22 illustrates the simulated elasto-plastic response of a single spudcan under vertical compression, on the same UWA sand (and MMC parameters) considered so far. Results are plotted after the initial pre-loading/unloading stage, that is starting from vertical load $V = V_{sw}$. As expected, the response of the footing features an elastic phase up to $V = V_0$, then new yielding gives rise to a non-linear hardening branch up to the ultimate plateau at $V = V_{lim} = 169$ MN (bearing capacity).

The same figure also reports the linear load-settlement behaviour (purple dashed line) associated with the ISO (2016) prediction of the vertical spudcan stiffness K_1:

$$K_1 = k_{d1}\frac{2GD}{1-\nu} \approx 2084 \text{ MN/m} \tag{10}$$

where G and ν are the shear modulus and the Poisson's ratio of the soil, D =10 m the embedded spudcan diameter, and k_{d1} a dimensionless stiffness coefficient – here taken as $k_{d1} = 1.16$ after setting (i) $\nu = 0.3$ (Table 2), (ii) full backfill and (ii) $2d/D \approx 0.5$ (d: embedment depth of the spudcan underside). The ISO standard recommends G values for sands based on the following equations:

$$\frac{G}{p_{atm}} = j\left(\frac{V_{sw}}{Ap_{atm}}\right)^{0.5} \approx 62.88 \text{ MPa} \tag{11}$$

$$j = 230\left(0.9 + \frac{D_r}{500}\right) \tag{12}$$

where in this case $p_{atm} = 101.3$ kPa (atmospheric pressure), $D_r = 84\%$ (relative density), A contact area and V_{sw} gross vertical spudcan reaction inclusive of backfill under still water conditions. Within the ISO framework the vertical stiffness K_1 depends linearly on the embedded diameter and the selected shear modulus, with the latter mainly affected by the initial contact pressure (V_{sw}/A) and only slightly by the relative density D_r (Equation (12)).

Although based on different arguments, the ISO prediction of G (Equation (11)) leads to a foundation stiffness in good agreement with what obtained through FE calculations and the calibrated MMC parameters in Table 2. Nonetheless, this comforting agreement seems insufficient to fully

capture the initial pushover stiffness of the whole jack-up. Reasons for such discrepancy most likely include installation effects overlooked in the (wished-in-place) FE model (and in the ISO standard as well), plus a quite simplistic modelling of the small-strain stiffness of the soil – a refined soil model and a wider set of lab test data at different confining pressures are expected to positively impact this issue.